J. Fluid Mech. (1967), *vol.* 28, *part* 4, *pp.* 803–821
Printed in Great Britain

A shear-free turbulent boundary layer

By T. UZKAN† AND W. C. REYNOLDS
Department of Mechanical Engineering, Stanford University

(Received 19 April 1966 and in revised form 17 October 1966)

A simple wall-turbulence interaction has been studied experimentally. In the idealized model an infinite flat plate is suddenly inserted into a pre-existing field of homogeneous isotropic turbulence, and subsequent changes in the turbulence field examined. The experiment involved passing grid-produced turbulence over a wall moving at the mean speed. Mean velocity gradients vanish in both the model and experiment, and hence production of new turbulence is absent. This allowed the inhibiting effects of the wall to be studied separately. The growth of the 'inhomogeneity layer' into the impressed turbulence field and other statistical features of the turbulence were measured.

1. Introduction

This paper deals with the interaction between a wall and a turbulent flow field. Previous studies of wall-bound and turbulent free shear layers suggest that the wall acts in two ways. First, the wall acts in a *direct* way, inhibiting the turbulent fluctuations in its vicinity. Secondly, the wall *indirectly* assists in the maintenance of mean velocity gradients which in turn interact with the turbulent fluctuations to produce new turbulence. Previous observations indicate that the outer (wake) portions of wall-bound turbulent shear layers are surprisingly similar to free turbulent shear layers. This suggests that the inhibiting action of the wall is not effective in the wake region, though it is clearly important close to the wall. Upon consideration of this state of knowledge, it appeared that a missing and needed study was one in which only the inhibiting effects of the wall were present. Such an investigation constitutes the work to be described.

The simplest type of free turbulence is that which can be idealized as motionless in the mean, and statistically both homogeneous and isotropic. This model has been used in previous investigations of the turbulence decay process. Now imagine that an infinite flat wall is suddenly placed in this infinite turbulence field. Initially the effects of the wall would be confined to a thin region near the surface, but this region would thicken in time and propagate into the turbulence field. Within this region the turbulence would no longer be isotropic but would be homogeneous in planes parallel to the wall. Since there would be no mean velocity gradients, no new turbulence would be produced, and hence the effect of the wall would be merely to alter the nature of the existing turbulence. The region of influence of the wall will be called the 'inhomogeneity layer'. This idealized type

† Present address: Yaver-Selahattin 10/4, Emirgan, Istanbul, Turkey.

of wall-turbulence interaction is the simplest conceivable, and forms a model for the present study.

The central objective of this research was the determination of the nature of the turbulence in the inhomogeneity layer, and the rate of growth of this layer into the external turbulence field. The program involved measurement and analysis of pertinent statistical properties of the turbulence, both within and external to the inhomogeneity layer, in an apparatus simulating the idealized situation.

While it is impossible to exactly produce homogeneous isotropic turbulence, the turbulence field produced by passing fluid through a grid has many features of such turbulence when viewed by an observer travelling downstream with the mean flow velocity. The sudden insertion of a wall can be accomplished by passing this flow stream over a wall moving at the mean velocity. Thus, an observer attached to the moving wall would see a growth of the inhomogeneity layer in time, essentially as in the model problem outlined above.

The present experimental program was conventional in concept but novel in execution. Whereas relatively standard grid-produced turbulence and hot-wire anemometry were employed, water (rather than air) was used as the working fluid for several reasons. It permitted low speed operation, which greatly simplified the design of the moving wall, and allowed desirable experimental conditions to be obtained with large-scale grids. Although the general approach to hot-wire operation in water had been developed previously, further refinement was necessary for the present experiments. Consequently a further improved constant temperature hot-wire system was developed. The fluctuation frequencies encountered in these low speed operations were so low that unconventional techniques for data recovery and processing were required. With the developed apparatus it was possible to measure a variety of statistical properties of the inhomogeneity layer. These included turbulence intensity profiles, spectra, and probability distributions associated with longitudinal fluctuations. The experimental system and the results obtained are reviewed in the following sections. For additional data and detail see Uzkan & Reynolds (1965).

2. Experimental techniques

(*a*) *Flow system*

The experiments were performed in an available water table which had the configuration shown in figure 1. The water was supplied from a circulation system capable of deaerating, filtering and deionizing the water. The details of the main circulation and associated subsystems are described by Runstadler, Kline & Reynolds (1963). The inlet nozzle shape and the number and location of the screens at the inlet and outlet of the channel were adjusted until an acceptably uniform flow at the grid was obtained. The flow rate and mean velocity were controlled by changing the height of a dam at the end of the water table.

The turbulence was created by a square mesh aluminum rod grid shown in figure 2. The grid mesh-length to rod-diameter ratio was chosen as 5·33 to allow comparison of the turbulence decay measurements with data available in the

literature. The choice of grid scale was based on a compromise between the desire for many bars and the difficulties of small scale and rapid decay associated with smaller rods.†

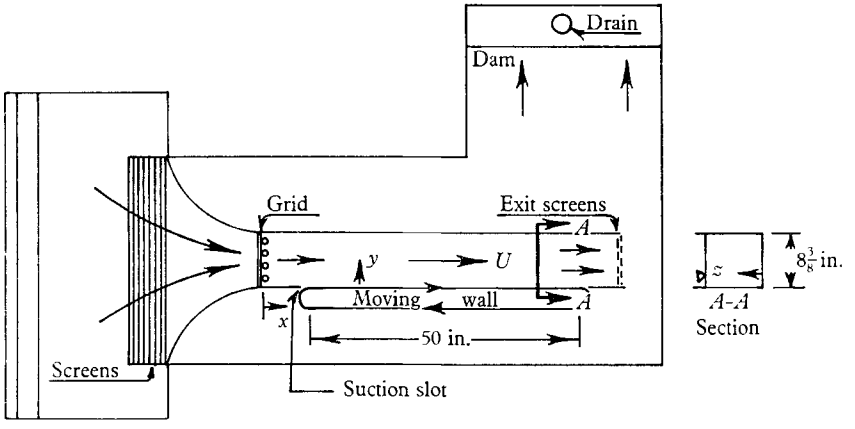

FIGURE 1. Schematic view of flow channel, plan view.

In order to match the wall speed with the free-stream speed, a continuous belt mechanism was built on one side of the channel, as shown in figure 3. The moving belt was cloth based rubber with dimensions $110 \times 10 \times \frac{1}{8}$ in. This belt provided a moving surface 50 in. long for full depth of the channel. The surface of the belt was hydraulically smooth, and the thickness variation of the belt was $\pm 0{\cdot}002$ in., except at the 45° lap joint where it was $\pm 0{\cdot}005$ in. The belt ran between two drums of $2\frac{7}{8}$ in. diameter. These drums were crowned inward for 0·25° and cross-knurled to prevent slippage. A careful test indicated no appreciable slip.

The belt was driven through a worm gear by a D.C. motor, which held the speed constant within 0·5%. The speed of the belt could be varied between 0·1–0·8 ft./sec in either direction. Vibrational disturbances of the driving unit were minimized through use of rubber pads and flexible couplings. To prevent sagging and vibration of the belt, a constant suction was applied to draw the belt against the front plate, and guide pieces were used to limit its vertical motion. A slight suction was applied where the belt fares into the stationary wall to counteract the convection of water by the moving wall surface. Two clearance vanes were used to control the suction flow rate, which was adjusted to provide a uniform flow downstream of the suction slot.

(*b*) *Hot-wire system*

Hot-wire operation in low velocity water flows presents several unusual problems (Sabin 1963), which necessitated development of a special anemometer. A schematic diagram of our constant-temperature linearized hot-wire anemometer is shown in figure 4. Its operating characteristics are outlined below:

probe overheat temperature range, 25–40 °F (30 °F used for the present data),

† While it may seem that the number of rods should have been greater, surveys of the turbulence field showed that a reasonable degree of homogeneity was obtained downstream in the test section (figure 13).

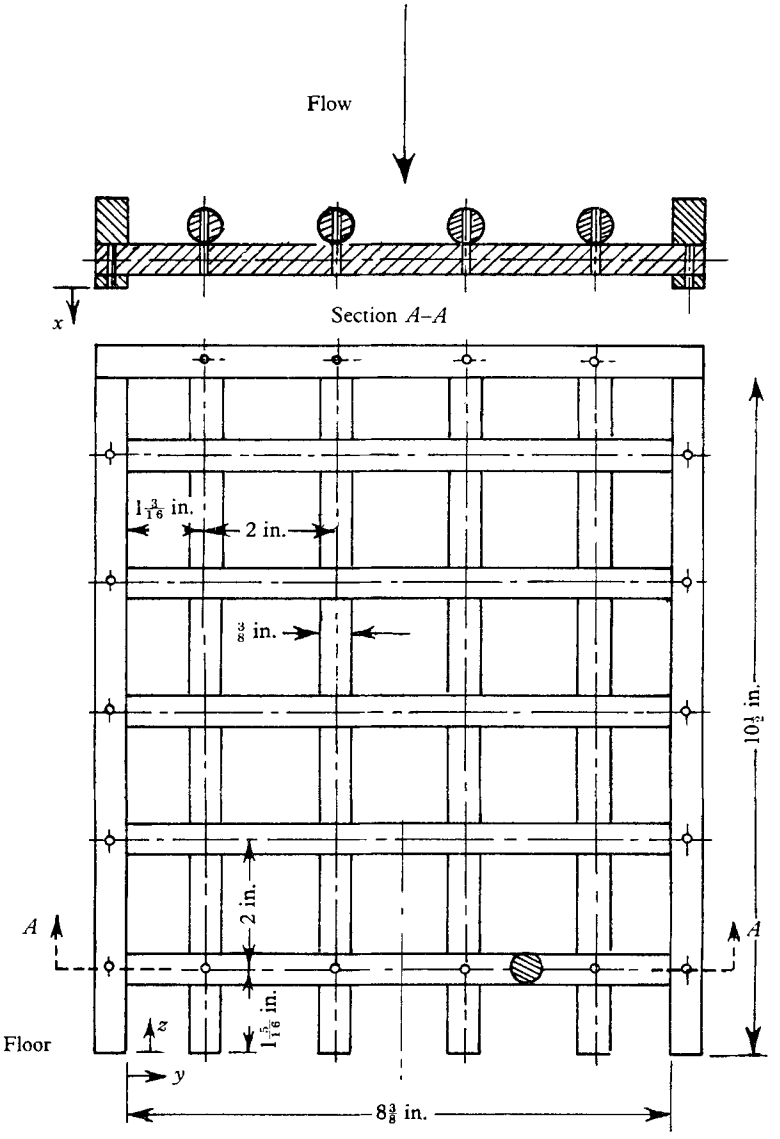

FIGURE 2. Details of the grid.

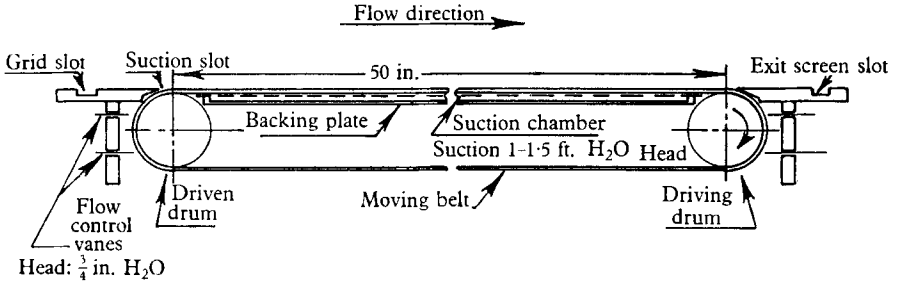

FIGURE 3. Schematic details of moving channel wall.

probe resistance range, 0·9–3·5 Ω,
drift, less than 1·5 %/hour,
frequency range, 0–800 c/s,
noise to signal ratio, less than 0·02–0·03 %,
noise to fluctuation signal ratio, less than 2 % for 2 % relative turbulence intensity,
power supply, batteries.

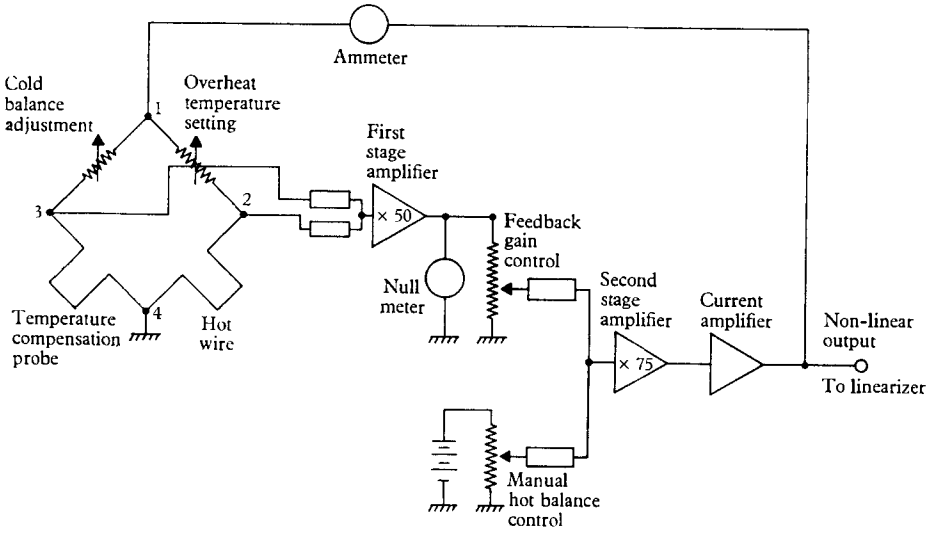

FIGURE 4*a*. Constant temperature hot-wire anemometer, schematic diagram.

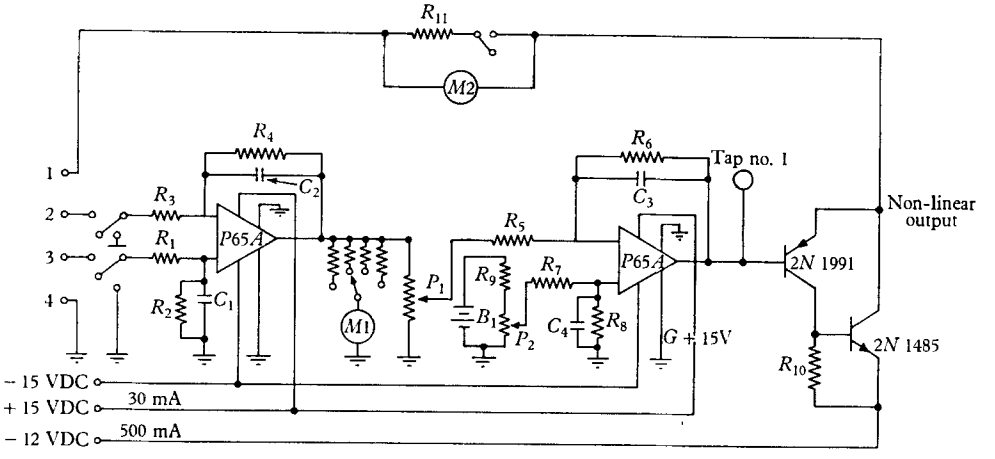

FIGURE 4*b*. Solid state amplifier details.

Component values:

$R_1 = R_3 = R_5 = R_7 = 20$ kΩ 1·0 %
$R_2 = R_4 = 1$ MΩ 1·0 %
$R_6 = R_8 = 1{\cdot}5$ MΩ 0·5 %
$R_9 = 5$ kΩ $\frac{1}{2}w$ 10 %
$R_{11} = 0{\cdot}26$ Ω Manganin wire
$R_{10} = 10$ kΩ$\frac{1}{2}w$ 10 %

$C_1 = C_2 = 200$ pf 10 % disc type
$C_3 = C_4 = 120$ pf 10 % disc type
$P_1 = 10$ kΩ w.w.
$P_2 = 5$ kΩ 10 turn, linear
$B_1 = 1{\cdot}4$ volts Mallory 2Mg

P65A: Philbrick D.C. operational amplifier
*M*1: Microammeter ∓ 25μA
*M*2: Milliammeter 0–50 mA

A sketch of a typical probe is in figure 5. For the present tests wires were made from 0·0008 in. diameter pure platinum wire, 0·08 in. long, and spot welded on pure platinum supports. The welds were covered by a thin layer of epoxy plastic for mechanical support of the joints, but the actual element was uncoated.

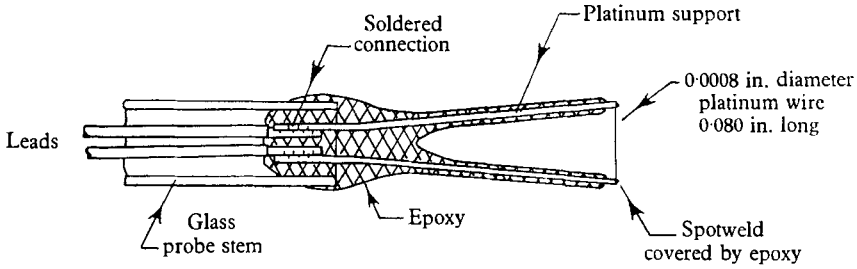

FIGURE 5. Construction details of hot-wire probes.

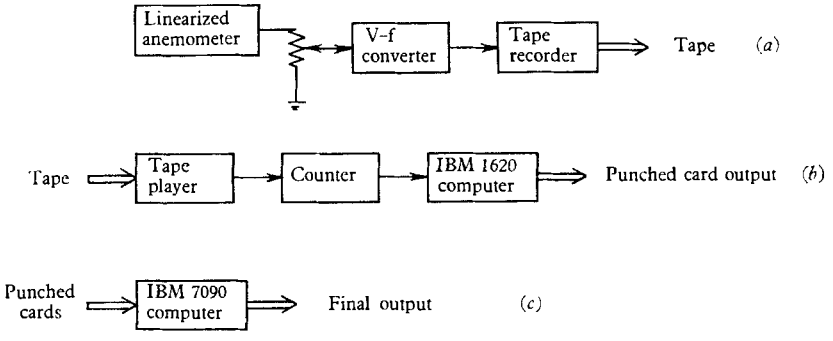

FIGURE 6. Digital data system.

(c) *Data acquisition and processing methods*

Two different schemes for data acquisition and processing were employed. The first involved obtaining digitized signals proportional to the average velocity over 10 millisecond intervals and processing by a digital computer. A separate electronic system provided for continuous analogue processing of the fluctuation signal. The digital system was used primarily to obtain information about the probability density and associated moments, and the analogue system was used for the spectral analysis.

The schematic diagrams for the digital system are shown in figure 6. The linearized anemometer output was converted to a frequency modulated high frequency (5–15 Kc) signal by a Vidar 240B voltage-to-frequency converter. This produced a frequency which was a linear function of the instantaneous velocity. The FM signal was then recorded on a home type Grundig AM TK-65 tape recorder. This system was used in a range where the distortion was less than 2 % and the linearity accurate to 1 %.

To obtain digitized data, the tape recorded signal was processed with the equipment shown in figure 6*b*. The counter determined the number of cycles recorded over a 10 ms time interval, and these numbers were punched on to cards. The sampling interval was chosen so that the maximum uncertainty (in

intensity) due to processing was less than 2%. The 10 ms sampling interval discards the spectral content above 100 c/s, and significantly alters the spectrum above about 20 c/s. Hence the digital scheme was *not* used to determine the spectra.

The schematic diagram of the analogue processing system is shown in figure 7. The principle element of this system is the Quantech model 304 spectrum analyzer,

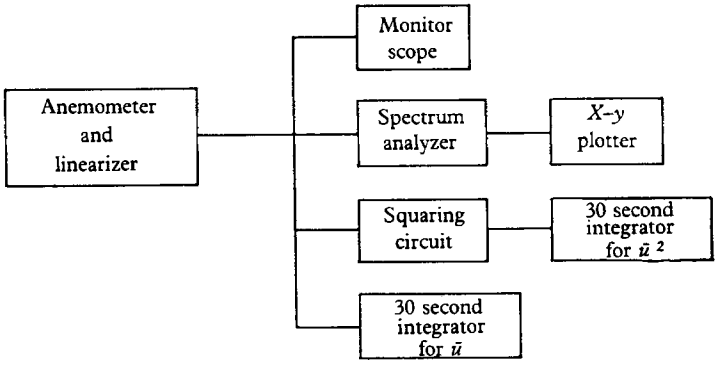

FIGURE 7. Analogue data system.

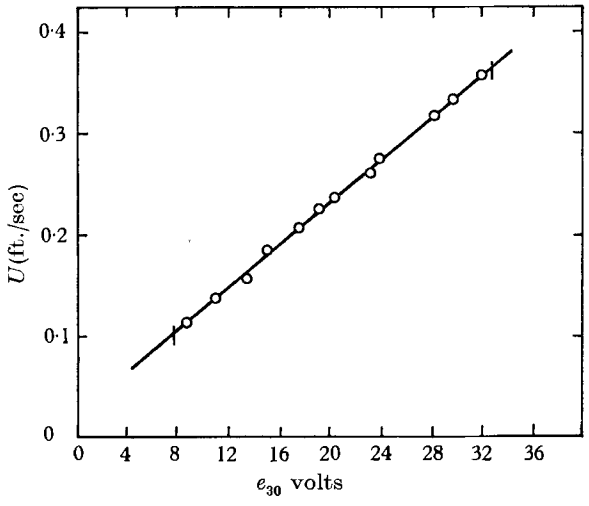

FIGURE 8. A typical hot-wire calibration.

$$e_{30} = k \int_0^{30} e\,dt$$

which is particularly well suited for turbulence measurements in water flows. It has a narrow band filter (1 c/s), is effective at relatively low frequencies (1 c/s), and provides automatic scanning. The data presented here were taken with 1 c/s filter bandwidth, 10 s meter time constant, 180 s sweep time, and 0–50 c/s sweep range. The analyzer output signal was recorded on 11 × 17 in. paper using an X-Y recorder. Several records were obtained at a given point in the flow field and averaged curves were drawn. Values read from the averaged curves at integer frequencies were used in subsequent calculations.

The mean velocity was obtained by integrating the linearized hot-wire signal for 30 s. The hot wires were calibrated in a steady laminar flow by measuring the vortex shedding rate from a small cylinder placed in front of the probe (Runstadler *et al.* 1963). A typical calibration is shown in figure 8.

(*d*) *Calculation of turbulence data*

The turbulence measurements were obtained from a hot-wire oriented perpendicular to the flow direction and parallel to the moving wall. As a first order approximation this wire measures the velocity component in the streamwise direction, $U_1(x)+u_1(x,t)$. Several kinds of turbulence information were obtained. Data presented here include the mean square turbulent fluctuation $\overline{u_1^2}$, which was obtained by digital processing of the digitized hot-wire signal. The one-dimensional spectral density was obtained from the frequency analysis of the hot-wire signal given by the spectrum analyzer. The spatial spectrum is proportional to the frequency spectrum, and the relation between spatial wave number k_1 and frequency f is taken as $k_1 = 2\pi f/U_1$. The constant of proportionality was determined from

$$\overline{u_1^2} = \int_0^\infty E_1(k_1)\,dk_1.$$

The integral scale (L) and microscale (λ) are

$$L = \int_0^\infty \hat{E}(r)\,dr,$$

$$\frac{1}{\lambda^2} = \frac{1}{2}\frac{\partial^2 \hat{E}}{\partial r^2}\bigg|_{r=0},$$

where $\hat{E}(r)$ is the Fourier transform of $E_1(k_1)$. These were computed from

$$L = \frac{U}{4\overline{u_1^2}} E_1(k_1)\bigg|_{k_1=0},$$

$$\lambda^2 = 2\overline{u_1^2}\left[\int_0^\infty k_1^2 E_1(k_1)\,dk_1\right]^{-1}.$$

The turbulence intensity and the microscale can be combined to give a *time scale for the turbulence*,

$$t_0 = \lambda(\overline{u_1^2})^{-\frac{1}{2}}.$$

Two thicknesses characterizing the inhomogeneity layer have been used. The *physical thickness* δ is arbitrarily taken where $\overline{u_1^2}$ is 99 % of its free-stream value. The physical thickness is difficult to measure accurately, and hence an integral thickness, the *energy deficit thickness*, Δ, was defined as

$$\Delta = \int_0^\infty [1-\overline{u_1^2}/(\overline{u_1^2})_\infty]\,dy.$$

Δ provides a measure of the depletion of turbulence energy brought about by the wall. A layer of the external turbulence field of thickness Δ would possess the same amount of turbulence energy in the u_1 component as is missing from the inhomogeneity layer.

3. Experimental results

(*a*) *Preliminary checks*

Prior to the turbulence experiments, the suitability of the basic flow was checked. The gross flow characteristics were checked by visual (dye injection) methods, and no secondary flows were observed. The water flow velocity was kept below

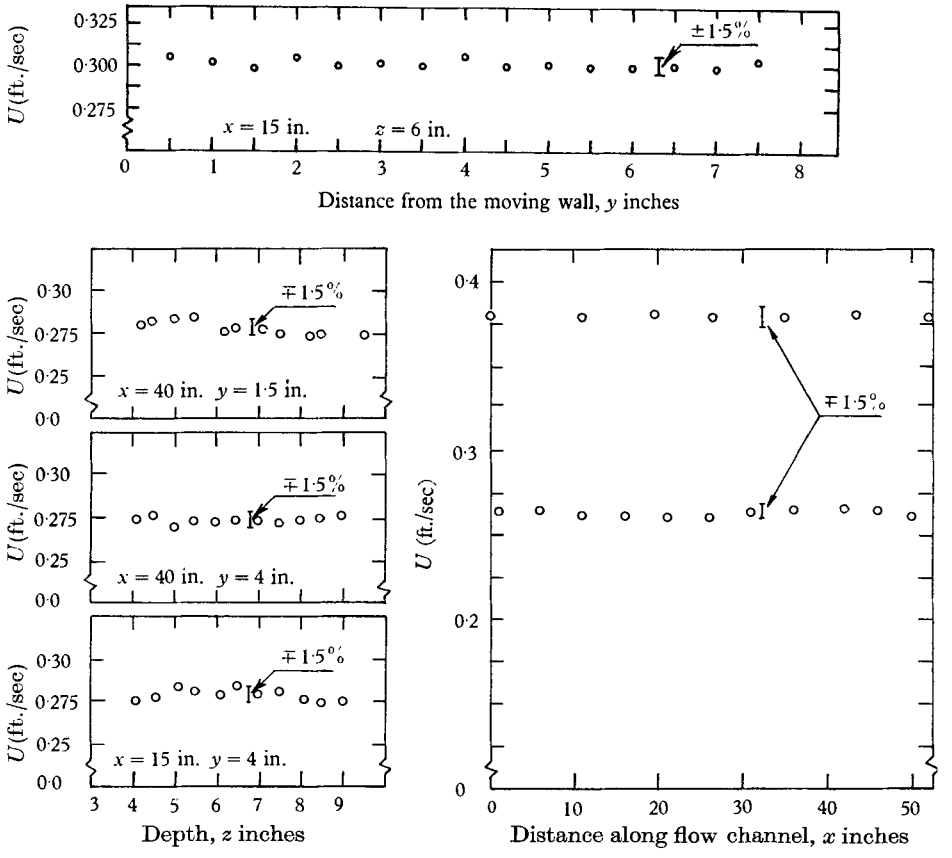

FIGURE 9. Some typical surveys of the flow channel without grid.

0·35 ft./sec in order to minimize exit disturbances and to keep the wake development region behind the grid within 15 in. Mean flow data in the channel were obtained by hot-wire measurements. Selected surveys from these measurements are presented in figure 9. Throughout the region of interest the mean velocity variation was less than 1·5 %, which was considered quite satisfactory. The wake development behind a grid bar is shown in figure 10. Note that the wake and jet effects are negligible after 14 in., and all subsequent turbulence data were taken downstream of this point. It is unfortunate that the problems of experimenting in low speed water flow made a critical examination of the homogeneity of the basic turbulence field difficult. Experience in air would suggest that a downstream distance of 40 meshes is required for satisfactory homogeneity. Hence perhaps the present results should be cautiously interpreted.

(b) Free-stream measurements

Initial experiments dealt with the decay of the grid-produced turbulence. Previous measurements of grid turbulence indicate that different periods of decay can be distinguished. The initial period can be identified as the region of decay where the turbulence energy varies approximately as t^{-1}, while in the final period the

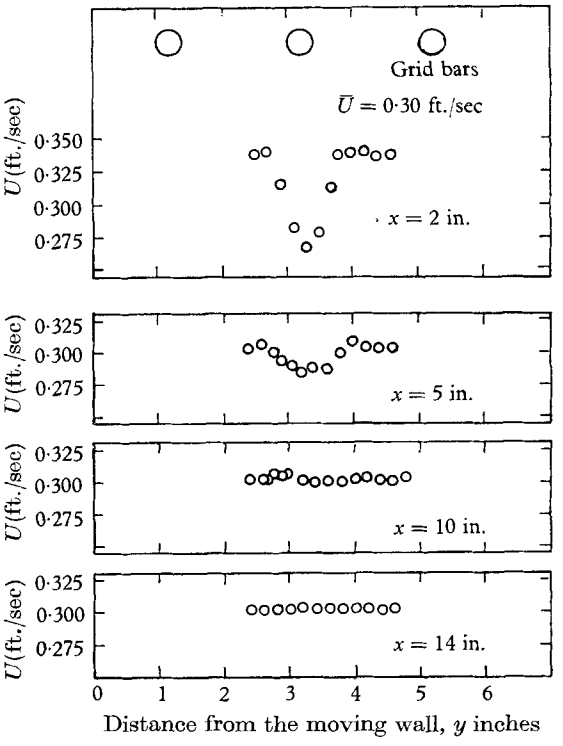

FIGURE 10. The development of the wake behind a grid bar.

energy varies as $t^{-\frac{5}{2}}$. A transition region blends these two modes of decay. For uniformly convected grid turbulence, the temporal decay appears as a streamwise reduction in the time-averaged properties.

Our data for decay behind the grid is presented in figures 11 and 12. Here the subscript ∞ indicates free-stream value. These data were taken with $U = 0{\cdot}305$ ft./sec along a streamline away from the wall. The variation of $\overline{u_1^2}$ is shown in figure 11, which suggests that the turbulence is in the initial period region for $12 < x < 40$ in. The x/M intercept of the best fit line to data is approximately at $x_0/M = 3{\cdot}0$. Corresponding intercepts obtained in previous measurements in wind tunnels give values between 10 to 20 (e.g. Batchelor 1953). The Townsend–Batchelor data taken with parameters $M/d = 5{\cdot}33$ and $Re_M = 5500$ are the closest to the present tests ($M/d = 5{\cdot}33$ and $Re_M = 5250$) and give a value $x_0/M = 15$–20. Batchelor suggested an initial period decay law of the form

$$\frac{U_1^2}{\overline{u_1^2}} = \frac{c}{C_D}\left(\frac{x}{M} - \frac{x_0}{M}\right),$$

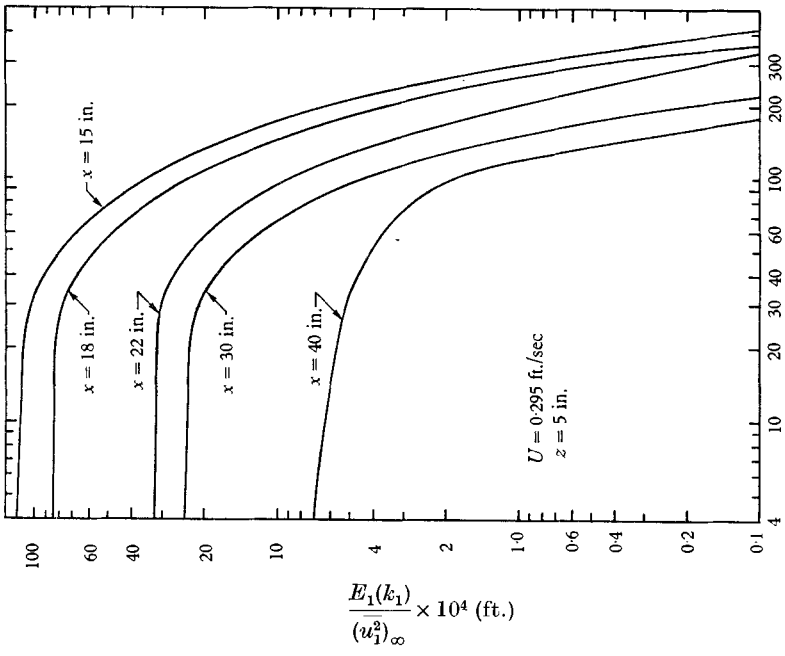

FIGURE 12. One-dimensional energy spectra in decaying turbulence.

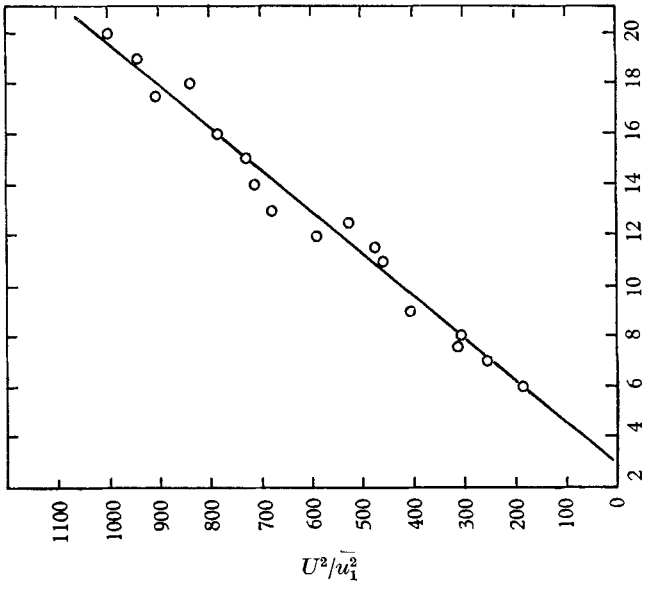

FIGURE 11. Decay of relative turbulence intensity in the flow channel. $U = 0{\cdot}305$ ft./sec; $M/d = 5{\cdot}33$; $Re_M = 5080$; $y = 4$ in.; $z = 4{\cdot}5$ in. Best fit line, $U^2/\overline{u_1^2} = 60(x/M - 3)$.

where C_D is the drag coefficient and c is a constant representing the effects of different geometries. The best fit to the present data is given by $c/C_D = 60$, $x_0/M = 3{\cdot}0$. The constant 60 is somewhat below the value of 135 which was suggested by Hinze (1959) on the basis of air experiments. Together with the lower value of x_0/M, the present tests indicate some differences between the present and previous data. Additionally, data taken beyond $x = 40$ in. indicated that the departure from the initial period behaviour began at about $x/M \approx 30$; in contrast, the expectation based on previous measurements (Hinze 1959) was that the initial period would extend somewhat further. No explanation for these differences can be given at this time, but it is known that the structure and decay of grid turbulence are very sensitive to the free-stream turbulence and grid configuration, and hence some seemingly unimportant factor may be responsible for the deviations from previous behaviour. But as the main purpose of these measurements was to establish the decay law outside of the inhomogeneity layer, this point was not pursued further.

Free-stream spectra are shown for several streamwise (x) stations in figure 12. The general behaviour is similar to that observed with air.

The data obtained in the free-stream have the same qualitative behaviour as previous experiments in air, though there are some quantitative differences. Hence it was felt that the present free-stream structure was adequately determined, though the degree of homogeneity in the turbulence field remains unresolved.

(c) *Inhomogeneity layer measurements*

The structure of the decaying turbulence is altered by the wall within the region which we have called the inhomogeneity layer. The extent of this layer can be obtained from inspection of the $\overline{u_1^2}$ profiles in figure 13. Note that the profiles are extremely smooth, and do not exhibit the characteristic peak found for boundary layers on stationary walls (Klebanoff 1954). This is an indication of the absence of any turbulence production. The intersection of the lines through the data with the lines marked Δ and δ indicate the values of the two thickness parameters defined previously.

The turbulence intensity variation with x at fixed y is shown in figure 14. Note that the decay is more rapid near the wall, but the free-stream behaviour is approached towards the outer edge of the inhomogeneity layer.

One-dimensional energy spectra are shown in figure 15 as functions of y at one x station.† The significant range of energy containing motions is covered by these curves, and hence the integrations required for normalization on $\overline{u_{1\infty}^2}$ are sufficiently accurate. As might be expected, the low wave number range shows the most pronounced wall influence and all wave numbers are attenuated by the presence of the wall. These curves suggest that different wave numbers have different thicknesses, with the inhomogeneity layer appearing thicker to larger scale motions. This is in qualitative agreement with the theory of Sternberg

† Note that the value of E_1 does not vanish for $k = 0$, since this is a one-dimensional spectrum.

(1962, 1965); it also agrees with Prandtl's mixing length ideas, which view the wall suppression as extending farther out for larger scale motions.

Figure 16 shows the distribution of the so-called 'dissipation integral' across the inhomogeneity layer. This integral provides a rough measure of the rate of

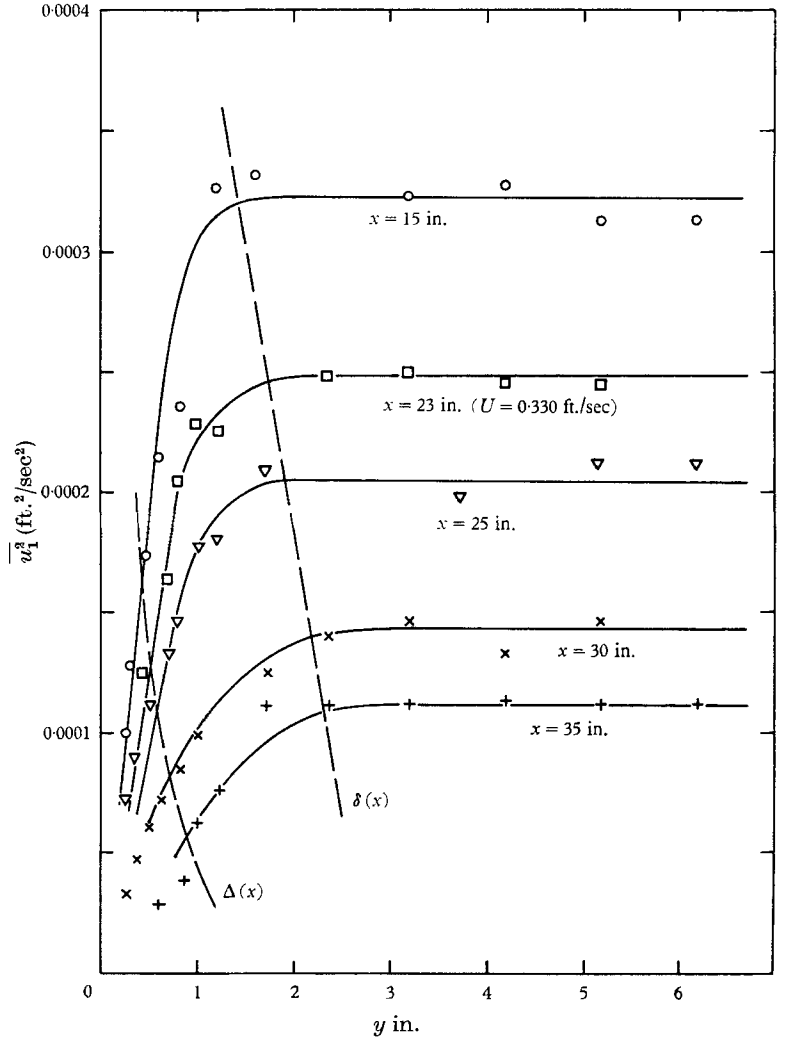

FIGURE 13. $\overline{u_1^2}$ Profiles in the inhomogeneity layer. U = 0·315 ft./sec; U_W/U = 1·0; M/d = 5·33; Re_M = 5250.

turbulent energy dissipation/unit of volume. The dissipation rate must vanish at the wall, and hence the integral is less in the inhomogeneity layer than in the free-stream. The turbulence time scale, microscale, and integral scales are shown as functions of y in figures 17 and 18. Note that the time scale increases towards the wall; the decrease of length scale towards the walls implies that the average eddy size is smaller near the wall. However, the effect of the wall on eddy size is

much less than the effect on the time scale, which suggests that the wall mainly slows down the turbulent motions while only slightly changing their physical scale.

(*d*) *Velocity mismatch data*

The data presented in the previous section dealt exclusively with the case where the wall speed was adjusted to match the free-stream speed as closely as possible. In order to evaluate the effect of imperfect velocity matching, some of the

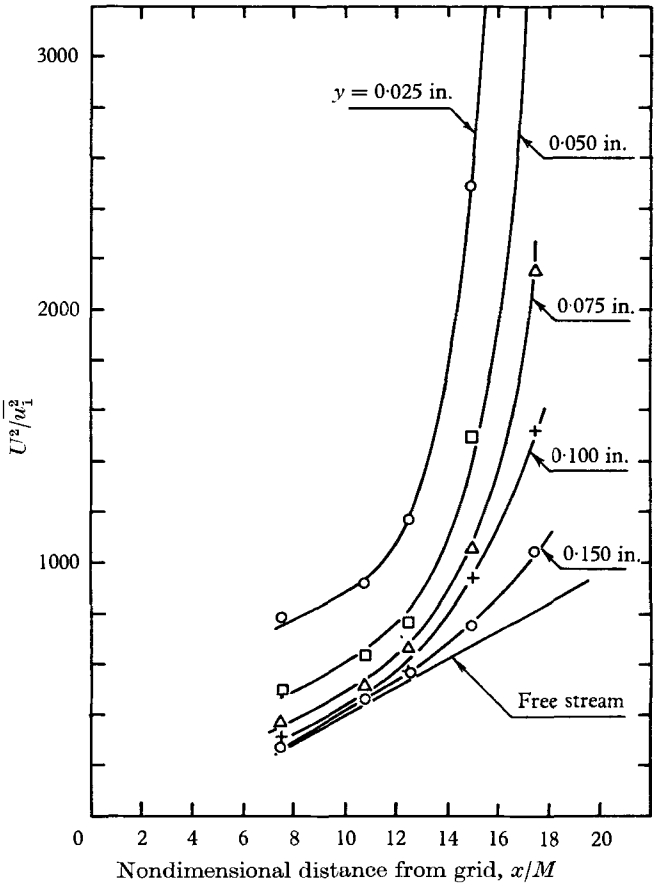

FIGURE 14. Decay of nondimensional turbulence intensity within inhomogeneity layer. U = 0·315 ft./sec; U_W/U = 1·0; M/d = 5·33; Re_M = 5250; z = 4·5 in.

experiments were repeated with the wall moving at 90 % of the free-stream speed ($U_W = 0{\cdot}9U_\infty$), and with the wall stationary. No attempt will be made to relate these data to previous boundary layer measurements, but a more extensive study along these lines is being contemplated as an extension of the present work.

The $\overline{u_1^2}$ and U_1 profiles for two values of U_W/U_∞ are shown in figures 19 and 20. Note that even a modest amount of mismatch introduces some turbulence production within the inhomogeneity layer. For the stationary wall case a very sharp peak occurs in the $\overline{u_1^2}$ profile near the wall.

It would appear from inspection of these data that a very slight mean velocity gradient would produce noticeable peaking in the intensity profile. Since none was observed, it is concluded that the velocity match was indeed satisfactory.

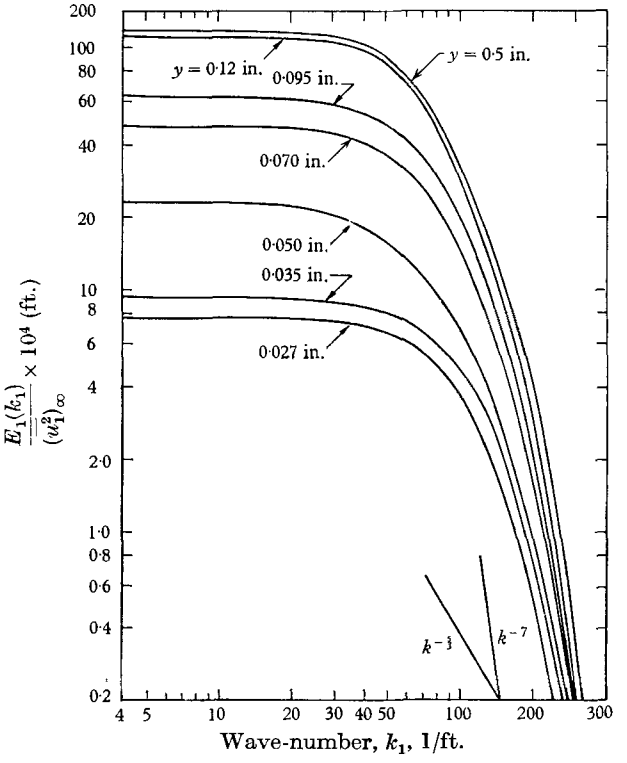

FIGURE 15. One-dimensional energy spectra in the inhomogeneity layer. $x = 15$ in.; $U = 0{\cdot}295$ ft./sec; $U_W/\bar{U} = 1{\cdot}0$; $z = 5$ in.

A simple visual study was made in addition to the main measurements. Using the dye-injection methods described by Runstadler *et al.* (1963), dye was placed on the moving wall, and the flow structure very near the wall was examined. When the turbulence grids were absent, and the wall was stationary, the streaky structure observed by Runstadler *et al.* in the wall layers of turbulent boundary layers was absent, indicating the presence of a laminar boundary layer. The streaks appeared when the grids were added, indicating that the boundary layer had become turbulent. Then, the wall speed was increased, until it matched the free-stream speed, at which point the streaks and the ejection of low speed fluid from the wall disappeared. When the wall was moved in the opposite direction, the streaky wall structure was replaced by a highly agitated turbulent structure, and the streaks were observed. The absence of streaks when $U_W = U_\infty$ strongly supports the hypothesis that the streaks and their breakup play a dominant role in the production of new turbulence.

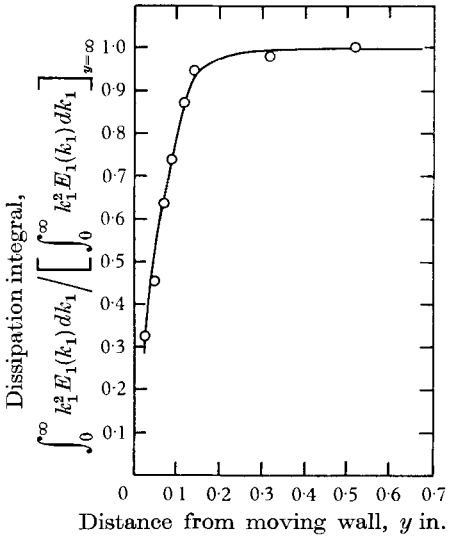

FIGURE 16. Dissipation integral in the inhomogeneity layer.
$x = 15$ in.; $\bar{U} = 0{\cdot}295$ ft./sec; $U_W/U = 1{\cdot}0$; $z = 5{\cdot}0$.

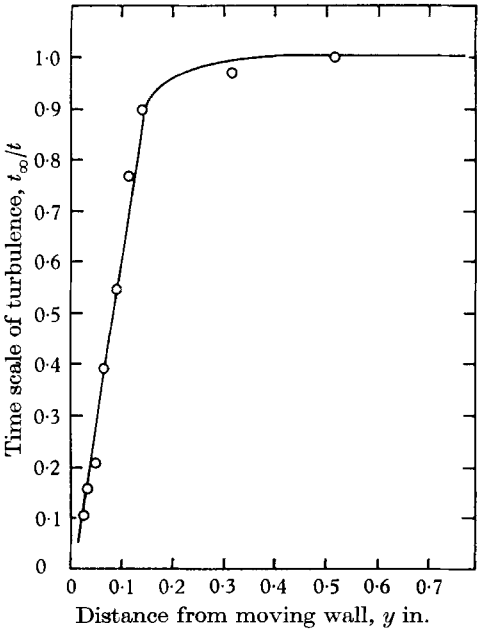

FIGURE 17

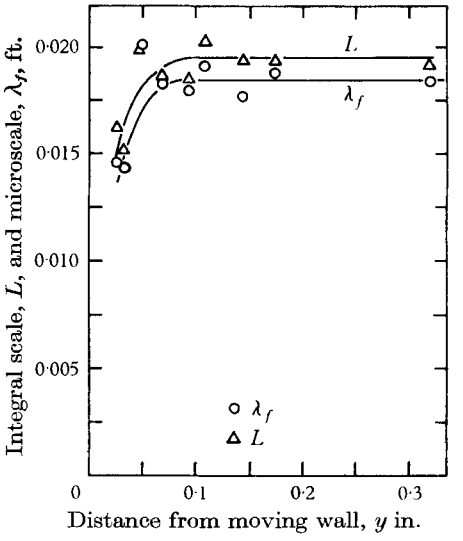

FIGURE 18

FIGURE 17. Time scale of turbulence in the inhomogeneity layer.
$x = 15$ in.; $U = 0{\cdot}295$ ft./sec; $U_W/U = 1{\cdot}0$; $z = 5$ in.

FIGURE 18. The integral and microscale of turbulence in the inhomogeneity layer.
$x = 15$ in.; $\bar{U} = 0{\cdot}295$ ft./sec; $U_W/U = 1{\cdot}0$; $z = 5$ in.

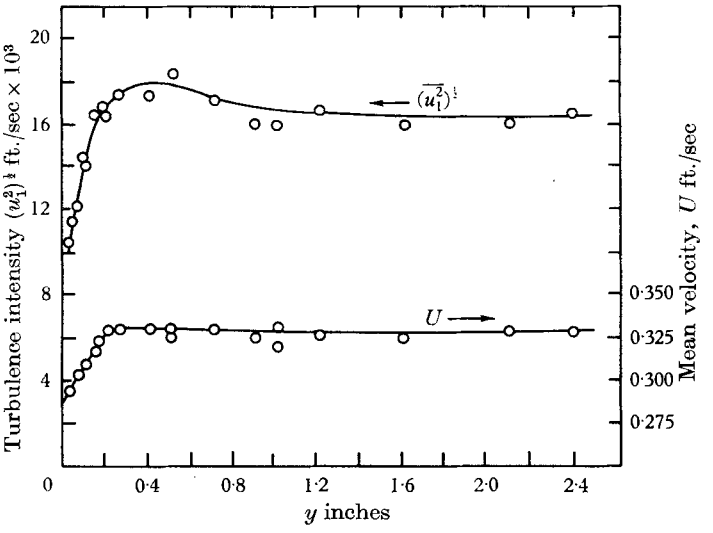

FIGURE 19. Mean velocity and intensity profile for 10 % velocity mismatch in moving wall speed. $U = 0{\cdot}330$ ft./sec; $x = 19$ in.; $U_W/U_\infty = 0{\cdot}90$.

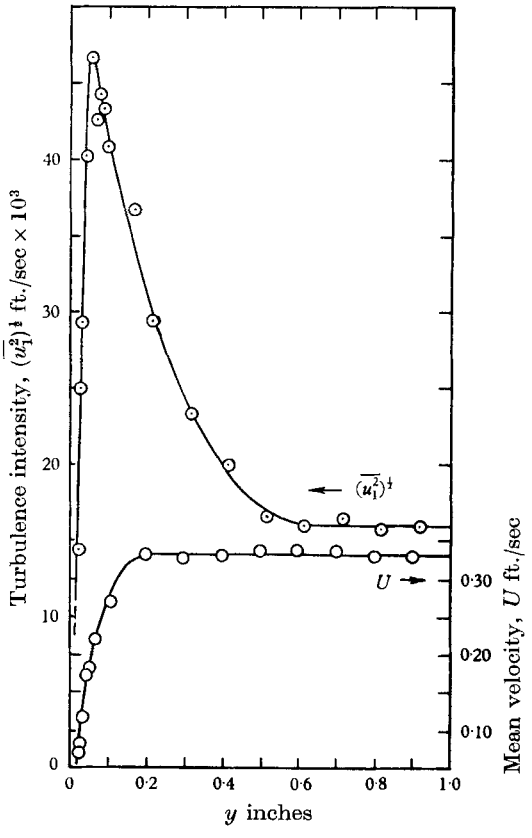

FIGURE 20. Mean velocity and turbulence intensity profiles on the stationary wall. $U = 0{\cdot}330$ ft./sec; $U_W/U_\infty = 0{\cdot}0$; $x = 19$ in.

4. Discussion

The primary objective of the present study was to learn how the wall alters the structure of turbulence nearby and the extent of the region of this influence into the impressed turbulence field. The experiments indicate that, in the absence of mean velocity gradients, the wall acts to attenuate the turbulence. The intensity profiles were quite smooth, and did not show the characteristic peak found when the wall is stationary.

The $E_1(k_1)$ spectra show that there is some slight preferential attenuation of low wave numbers, indicating that the wall is more efficient in damping larger eddies. Furthermore, the distance from the wall which is influenced by the wall seems slightly greater for large eddies, though the spread is not great over the range of energy-containing wave numbers. No really drastic changes in the spectra were observed, and the variations throughout the inhomogeneity layer are quite smooth.

u_2 or u_3 fluctuations were not measured, but some speculation about their general behaviour can be made. It is expected that the impervious nature of the wall acts to attenuate u_2 fluctuations most rapidly, as only viscous effects attenuate u_1 and u_3 fluctuations. Thus, the energy deficit thickness for u_2 fluctuations is probably somewhat greater than that measured for u_1.

The extent to which the inhibiting wall effects extend into the field of impressed turbulence is of particular importance, since this is expected to be roughly applicable within turbulent shear layers. Based on the present experiments, we can estimate the inhomogeneity layer thickness roughly as

$$\delta \approx 1{\cdot}83(\nu/U_\infty)^{0{\cdot}5}x^{0{\cdot}5},$$

where x represents the distance from the start of the layer, and U_∞ is the free-stream velocity. For comparison, the thickness of a turbulent boundary layer on a flat plate is given approximately by (Eckert & Drake 1959)

$$\delta_{tb} = 0{\cdot}376(\nu/U_\infty)^{0{\cdot}2}x^{0{\cdot}8}.$$

Assuming (with no particular justification) that the order of magnitude of the direct wall influence is unchanged by the presence of turbulence production (which occurs mainly in a thin region very close to the wall), the inhibiting wall effects would extend over only about 10 % of the turbulent boundary layer for a flow with $xU_\infty/\nu = 10^6$ and over only 5 % of the boundary layer at $xU_\infty/\nu = 10^7$. This observation may well explain why the structure of the turbulence in the outer portion of a turbulent boundary layer bears so much resemblance to the turbulence in free turbulent shear layers.

The support of this work by the National Science Foundation and the Air Force Office of Scientific Research is gratefully acknowledged. We are deeply indebted to Professor S. J. Kline, who made many valuable suggestions during the course of this study, and to a referee for most helpful and educational criticisms of an earlier manuscript.

REFERENCES

BATCHELOR, G. K. 1953 *The Theory of Homogeneous Turbulence.* Cambridge University Press.

ECKERT, E. R. G. & DRAKE, R. M. 1959 *Heat and Mass Transfer.* New York: McGraw-Hill.

HINZE, J. O. 1959 *Turbulence.* New York: McGraw-Hill.

KLEBANOFF, P. S. 1954 *NACA TN* 3178.

RUNSTADLER, P. S., KLINE, S. J. & REYNOLDS, W. C. 1963 *Thermosciences Div., Mech. Engng. Dept., Stanford University, Rept.* MD-8.

SABIN, C. M. 1963 *Thermosciences Div., Mech. Engng. Dept., Stanford University, Rept.* MD-9.

STERNBERG, J. 1962 *J. Fluid Mech.* **13**, 241.

STERNBERG, J. 1965 *Agardograph* 97, Part 1.

UZKAN, T. & REYNOLDS, W. C. 1965 *Thermosciences Div., Mech. Engng. Dept., Stanford University, Rept.* MD-14.

CORRIGENDUM

'Hydromagnetic stability of dissipative flow between rotating permeable cylinders. Part 1. Stationary critical modes', by TIEN SUN CHANG and WALTER K. SARTORY, *J. Fluid Mech.* vol. **27**, 1967, p. 65.

The symbols of the abscissae and ordinates should be interchanged in figures 1–4, 6, and B_2 should be β_2.